

OPTICAL/SAR SENSORS STEREO POSITIONING

Shuai Xing*, Qing Xu, Yan Zhang, Yu He, Guowang Jin

Zhengzhou Institute of Surveying and Mapping, 450052 Zhengzhou, China - xing972403@163.com

Commission I, ICWG I/V

KEY WORDS: Accuracy, Mapping, Orientation, Optical, Photogrammetry, Stereoscopic, SAR

ABSTRACT:

Up till now it is still difficult to acquire stereoscopic space-borne image pairs of some area due to climate condition or atmosphere pollution. This paper describes the geometric aspects and the mathematical treatment for the stereoscopic image pair composed of optical and SAR space-borne images in positioning. First, the geometric equation for linear array push-broom imagery and F. Leberl model for SAR imagery as well as methods to simultaneously determine or refine individual parameters of these models are briefly reviewed. And a straight-forward single-step procedure has been developed which follows the philosophy of photogrammetric bundle adjustment techniques. Secondly, from these imaging models of one optical and SAR image, the composite stereoscopic pair is constructed. The stereo positioning is the process of determining the ground coordinate of a ground point from a pair of homologue points in the composite stereoscopic pair. Experimental results show that it is feasible to construct stereoscopic pair with one optical and SAR image, of which the average positioning RMS value is close to stereoscopic pair with optical/optical or SAR/SAR images.

1. INTRODUCTION

High resolution optical stereoscopic image pairs achieved by some commercial remote sensing satellites, such as IKONOS, SPOT5, Quickbird etc, have been widely used to produce medium and large scale cartography. But until now it is difficult to acquire satisfied optical space-borne image of some area, like basin or tableland, for complicated climate or serious atmosphere pollution. Radargrammetry is a good solution to this problem, but the stereoscopic observation and interpretation of SAR stereoscopic image pair are extremely rigorous. So this paper describes another solution as Figure 1, which constructs a stereoscopic pair with optical/SAR space-borne images for stereo positioning.

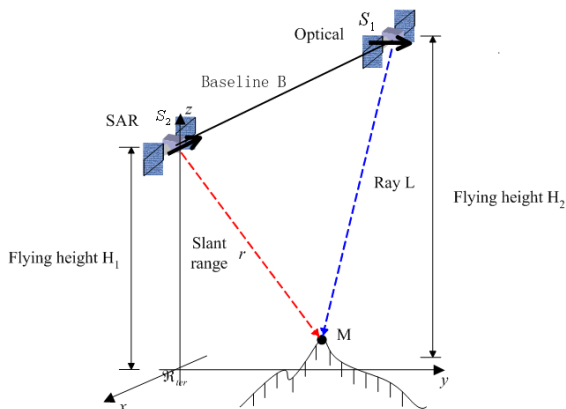


Figure 1. Scheme of a multi-sensor stereo positioning

After Moore first proposed the stereoplottting based on the stereoscopic pair with SAR and optical images in 1970, lots of works on theory have been done in the past twenty years. In 1990 Johannes Raggam and Alexander Almer (Raggam Johannes et al., 1990) of institute for image processing and computer graphics in Austria have analyzed the geometric aspects and the mathematical treatment of stereoscopic pair composed of optical and SAR space-borne images, and have

chosen a Seasat SAR image, SPOT image and Landsat TM image to construct three stereoscopic pairs. Accuracies of stereo positioning are that planimetric error is 28-45m and altimetric error is 14-30m. In the middle of 1990s, two satellites, ERS-1 and Radarsat-1, have been launched successfully and high resolution SAR images could be acquired. And the high accuracy of composite positioning has been achieved too. In 1993 Renouard and Perlant (Renouard L., 1993) combined SPOT and ERS image to achieve planimetric error 15m and altimetric 10m. In 1994 Toutin chose Radarsat, RSO-C/X, ERS, SPOT and Landsat TM images, and stated planimetric errors around 15m and altimetric around 20m. In 2004 Alain Giros of ESA tried to auto register and composite position SPOT and ERS-2 images to achieve planimetric error 10-40m and altimetric 10-17m. (Jordi Inglada et al., 2004; Alain Giros, 2005) In 2006 Fang Yong et al. (Fang Yong et al., 2006) tried to stereoplottting with Radarsat-1 and ERS-2 stereoscopic pair based on G. Konecny model and achieved planimetric error 34.24m and altimetric 14.08m.

In this paper the stereoscopic pair composed of linear array push-broom and SAR space-borne images is discussed, its construction and procedure of stereo positioning are described in details. First the imaging models for linear array push-broom imagery and SAR imagery are introduced in section 2. Then the mathematical treatment of composite stereoscopic pair is constructed in section 3. Section 4 shows experimental results with six stereoscopic pairs and section 5 shows conclusions.

2. TWO IMAGING MODELS

2.1 The Scanning Model

The linear array push-broom imagery is acquired with linear sensors by scanning the Earth surface. The relationship between ground and image is rigorous central projection. Each line of the image has different elements of exterior orientation. The collinearity equation of i line is expressed in the following way: (Qian Zengbo et al., 1992; Chang Benyi, 1989; Yan Qin et al., 2001)

$$\left. \begin{aligned} x_i &= -f \frac{a_1(X - X_{si}) + b_1(Y - Y_{si}) + c_1(Z - Z_{si})}{a_3(X - X_{si}) + b_3(Y - Y_{si}) + c_3(Z - Z_{si})} \\ 0 &= -f \frac{a_2(X - X_{si}) + b_2(Y - Y_{si}) + c_2(Z - Z_{si})}{a_3(X - X_{si}) + b_3(Y - Y_{si}) + c_3(Z - Z_{si})} \end{aligned} \right\} \quad (1)$$

Where a_i, b_i, c_i ($i=1,2,3$) are elements of rotation matrix composed of $\varphi_i, \omega_i, \kappa_i$, which are angle elements of exterior orientation.

Two observation equations can be constructed with one ground control point (gcp). So at least 6 gcps and satellite orbit parameters are needed to achieve elements of exterior orientation of linear array push-broom imagery.

2.2 F. Leberl Model

The geometry relation between ground and image points in a SAR image is established by the Doppler and Range equations proposed by F. Leberl. (Xiao Guochao et al., 2001; He Yu, 2005)

The range equation of slant range image is

$$(X - X_s)^2 + (Y - Y_s)^2 + (Z - Z_s)^2 = (y_s M_y + D_{s_0})^2 \quad (2)$$

Where D_{s_0} is the slant range delay, y_s is the across-track image coordinate of ground point P, M_y is the across-track pixel size, (X, Y, Z) are the object space coordinates of ground point P, (X_s, Y_s, Z_s) are the object space coordinates of radar antenna center.

The Doppler equation is

$$Xv(X - X_s) + Yv(Y - Y_s) + Zv(Z - Z_s) = -\frac{\lambda R_s}{2} f_{DC} \quad (3)$$

Where R_s is the slant range of ground point P, λ is the radar wavelength, f_{DC} is the Doppler frequency.

F. Leberl model is composed of formula (2) and (3). When $f_{DC} = 0$, they can be linearized to achieve elements of exterior orientation with gcps.

3. THE CONSTRUCTION OF COMPOSITE STEREO MODEL

3.1 The Construction of Composite Stereoscopic Pair

There usually are two ways to construct stereoscopic pair. One is first relative orientation with connection points and then absolute orientation with gcps. The other is direct exterior orientation of two images respectively and then combination of them. Since the equations of relative orientation are derived from collinearity equations, the former way is invalid for SAR image. In the later way, the orientation procedure of two images can be applied with two different groups of gcps respectively, which avoids the difficulty for collecting connection points. Here we choose the later way to construct the composite stereoscopic pair.

As shown in (1), the exterior orientation elements of different line in linear array push-broom imagery are different. But

because imaging time of each line is very short, the correlation of the exterior orientation elements of different lines is inevitable, which might induce no solution for collinearity equations. The ridge estimation has been used for solving this problem, but it is difficult to choose ridge estimation parameters in the classical ridge estimation algorithms. Zhang Yan et al. (Zhang Yan et al., 2004) proposed a robust combined ridge with shrunken estimator (RCRS), which could improve complex collinearity of coefficient matrix and detect singularity of observed value, making the estimator optimal and stable. Here we used this algorithm to orient SPOT image and achieved sub-pixel RMS error.

In (3) for airborne SAR image, f_{DC} is approximately zero for earth's rotation. But for spaceborne SAR image, f_{DC} is not approximately zero but a linear function with time since flight height is higher. Because y_s linearly varies with time, f_{DC} can be expressed as a n -order polynomial with y_s . (Wang Donghong et al., 2005; Chen Puhuai et al., 2001) Then (3) can be written as

$$\begin{aligned} Xv(X - X_s) + Yv(Y - Y_s) + Zv(Z - Z_s) \\ = a_0 + a_1 y_s + a_2 y_s^2 + a_3 y_s^3 + a_4 y_s^4 \end{aligned} \quad (4)$$

Where a_i ($i=0,1,2,3,4$) are polynomial coefficients.

When the exterior orientation elements of linear array push-broom imagery and SAR image have been achieved respectively, the stereoscopic pair is constructed. The space coordinate of ground point can be computed with homologous image points based on space intersection.

3.2 Space Intersection

A procedure in the composite stereo positioning is the determination of object space coordinates X, Y, Z from a pair of homologous image points $(x_1, y_1; x_2, y_2)$ measured in both images of a stereo model. Using these measurements as input to the appropriate pair of mapping equations (i.e. equation (1) and (2) (4)) yields 4 equations to calculate 3 unknown entities.

The overdetermined problem is solved by standard least squares adjustment using equation (1) and (2) (4) to calculate proper increments to the approximations given for the unknown coordinates. Using equation (1) and (2) (4), the corresponding position equation is as follows (in matrix notation):

$$\mathbf{V} = \mathbf{D}\mathbf{\Delta} - \mathbf{L} \quad \mathbf{P} \quad (5)$$

The residual error vector is $\mathbf{V} = (v_1 \ v_2 \ v_3 \ v_4)^T$;

The coefficient matrix is

$$\mathbf{D} = (D_1 \ D_2 \ D_3 \ D_4)^T = \begin{pmatrix} d_{11} & d_{12} & d_{13} \\ d_{21} & d_{22} & d_{23} \\ d_{31} & d_{23} & d_{33} \\ d_{41} & d_{24} & d_{43} \end{pmatrix};$$

The increments vector of the unknown ground coordinates is

$$\mathbf{\Delta} = (dX \ dY \ dZ)^T;$$

The absolute term is $\mathbf{L} = (l_1 \ l_2 \ l_3 \ l_4)^T$;

The weight matrix is
$$\mathbf{P} = \begin{pmatrix} p_{x_1} & 0 & 0 & 0 \\ 0 & p_{y_1} & 0 & 0 \\ 0 & 0 & p_{x_2} & 0 \\ 0 & 0 & 0 & p_{y_2} \end{pmatrix};$$

After the manipulations, (5) can be written as

$$\mathbf{\Lambda} = (\mathbf{D}^T \mathbf{P} \mathbf{D})^{-1} \cdot \mathbf{D}^T \mathbf{P} \mathbf{L} \tag{6}$$

X, Y, Z can be achieved by this equation.

\mathbf{D} and \mathbf{L} in (5) and (6) are different with different stereoscopic pair. For example with SPOT and Radarsat-1 slant range images, the parameters of \mathbf{D} and \mathbf{L} are

$$\left\{ \begin{array}{l} d_{11} = C_{14} = \frac{1}{Z}(a_3 x_1 + f a_1) \\ d_{12} = C_{15} = \frac{1}{Z}(b_3 x_1 + f b_1) \\ d_{13} = C_{16} = \frac{1}{Z}(c_3 x_1 + f c_1) \\ d_{21} = C_{24} = \frac{f a_2}{Z} \\ d_{22} = C_{25} = \frac{f b_2}{Z} \\ d_{23} = C_{26} = \frac{f c_2}{Z} \end{array} \right. \quad \left\{ \begin{array}{l} d_{31} = A_{10} = -2(X - X_s) \\ d_{32} = A_{11} = -2(Y - Y_s) \\ d_{33} = A_{12} = -2(Z - Z_s) \\ d_{41} = A_{20} = X_v \\ d_{42} = A_{21} = Y_v \\ d_{43} = A_{22} = Z_v \end{array} \right.$$

$$\left\{ \begin{array}{l} l_1 = x_1 + f \frac{a_1(X - X_{si}) + b_1(Y - Y_{si}) + c_1(Z - Z_{si})}{a_3(X - X_{si}) + b_3(Y - Y_{si}) + c_3(Z - Z_{si})} \\ l_2 = 0 + f \frac{a_2(X - X_{si}) + b_2(Y - Y_{si}) + c_2(Z - Z_{si})}{a_3(X - X_{si}) + b_3(Y - Y_{si}) + c_3(Z - Z_{si})} \\ l_3 = (X - X_s)^2 - (Y - Y_s)^2 - (Z - Z_s)^2 \\ \quad - (y_2 M_y + Ds_0)^2 \\ l_4 = (a_0 + a_1 y_2 + a_2 y_2^2 + a_3 y_2^3 + a_4 y_2^4) \\ \quad - X_v(X - X_s) + Y_v(Y - Y_s) + Z_v(Z - Z_s) \end{array} \right.$$

4. EXPERIMENTS

4.1 Test Data

Four space-borne images covering an area in Beijing, China are chosen. The statistics of their attributes are shown in table 1. The overlap of four images is shown in Figure 2. The overlap of these images is up to 50%-100%. 30 gcps and 34 check points are manually collected in 1:25000 raster graphic and marked with blue triangles and green circles in Figure 2 respectively. The center of Beijing city, the Imperial Palace, is marked with a red pentacle in Figure 2. Especially, there are 6 gcps and 9 check points beyond the SPOT4 image, which are not used in any computation about the SPOT4 image for ensuring the reliability and accuracy of results.

4.2 Test Results

In this experiment, six composite stereoscopic pairs have been constructed, which are Radarsat1-ERS2, Radarsat1-SPOT4, SPOT4-ERS2, SPOT5-ERS2, SPOT5-Radarsat1 and SPOT5-SPOT4. Gcps are used to finish the orientation of the images and check points are used to check the stereo position accuracy of six composite stereoscopic pairs.

The statistics of RMS values of six pairs are shown in table 2. The absolute values of maximum and minimum residual error are also listed. In table 2, planimetric RMS error values are 10-26m and altimetric RMS error values are 15-28m. It means that the stereo position with composite stereoscopic pairs is

successful, and its accuracy is equivalent to the stereoscopic pair with optical/optical or SAR/SAR images.

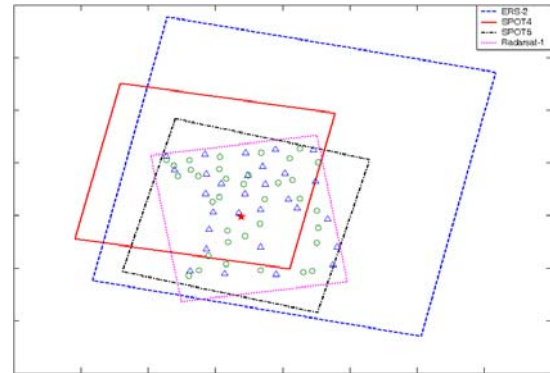


Figure 2. Overlap of four space-borne images and distribution of ground control points

The statistics of some attributes including overlap, intersection angle, length of baseline, flying height and base-height ratio are listed in table 3 for analyzing the relation between structure of the stereoscopic pair and the space intersection accuracy.

Experiment results in table 2 show that planimetric error of the composite stereo position is mainly determined by geometry condition of optical image. The planimetric error values of the stereoscopic pairs without optical images, such as Radarsat1-ERS2, are lower, but those of the stereoscopic pairs with optical images are better. And the spatial resolution of the optical image is higher, the composite stereo position accuracy is better. Obviously planimetric error values of the stereoscopic pairs with the SPOT-5 image are lower than other stereoscopic pairs with the SPOT-4 image.

Experiment results in table 2 also show that altimetric error of the composite stereo position is mainly determined by geometry condition of SAR image. In 6 stereoscopic pairs, the altimetric error value of Radarsat1-ERS2 is lowest, and that of SPOT5-SPOT4 is highest. And we find the intersection angle and base-height ratio of SPOT4-ERS2 are lowest in table 3, but its altimetric error value is not highest.

And altimetric error of the composite stereo position is secondarily determined by intersection geometry condition of the stereoscopic pair. In the stereoscopic pairs except Radarsat1-ERS2 and SPOT5-SPOT4, altimetric error of Radarsat1-SPOT4 is lowest and SPOT4-ERS2 is highest. In table 3, the intersection angle and base-height ratio of Radarsat1-SPOT4 are highest, but those of SPOT4-ERS2 are lowest.

5. CONCLUSIONS

The geometric aspects and the mathematical treatment for the stereoscopic image pair composed of linear array push-broom and SAR space-borne images have been introduced in this paper. And the geometric equations of the composite stereoscopic image pair are deduced in details. Experiment results demonstrate that it is feasible to construct stereoscopic pair with optical/SAR images, of which the mean RMS value is close to stereoscopic pair with optical/optical or SAR/SAR images.

This stereo model provides a new way to process multi-sensor satellite remote sensing images and can be used in key object position in remote sensing reconnaissance and stereoplotting in special areas. Since residual error of the homologous image point promulgates to the ground point coordinate, high accurate auto registration algorithm is a key point in our future work.

References

Alain Giros, http://earth.esa.int/rtd/Events/ESA-EUSC_2005 (accessed 20 Oct. 2005)

Chang Benyi, 1989. The preliminary research on stereo plotting method of spot imagery, *Agta Geodetica et Cartographica Sinica*, 18(3), pp. 183-189.

Chen Puhuai and Dowman Ian J., 2001. A weighted least squares solution for space intersection of spaceborne stereo sar data, *IEEE Transactions on Geoscience and Remote sensing*, 39(2), pp. 233-240.

Fang Yong, Chang Benyi, Hu Haiyan and Chen Hong, 2006. The research on sar image digital mapping technique, *Bulletin of Surveying and Mapping*, (8), pp. 6-8.

He Yu, 2005. SAR digital block triangulation, Master Thesis, *Zhengzhou Institute of Surveying and Mapping*, pp. 7-9.

Jordi Inglada and Alain Giros, 2004. On the possibility of automatic multisensor image registration, *IEEE Transactions on Geoscience and Remote sensing*, 42(10), pp. 2104-2120.

Qian Zengbo, Liu Jingyu and Xiao Guochao, 1992. *Space Photogrammetry*, PLA Press, pp. 152-155.

Raggam Johannes and Almer Alexander, 1990. Mathematical aspects of multi-sensor stereo mapping, *Proceedings of IGARSS'90*, Washington D.C., 3.

Renouard L. and F. Perlant, 1993. Geocoding SPOT Products with ERS-1 Geometry. *Proceedings of the Second ERS-1, Space at the Service of the Environment*, Hamburg, pp. 653-658.

Wang Donghong, Liu Jun and Zhang Li, 2005. Precise rectification of space-borne SAR images based on improved f. leberl model, *Bulletin of Surveying and Mapping*, 10, pp. 12-15.

Xiao Guochao and Zhu Cai-ying, 2001. *Radargrammetry*, Earthquake Press, pp. 56-58.

Yan Qin, Zhang Zuxun and Zhang Jianqing, 2001. Orientation of remote sensing images taken by ccd from different orbit, *Geomatics and Information Science of Wuhan University*, 26(3), pp. 270-274.

Zhang Yan, Wang Tao, Zhu Shulong and Zhu Baoshan, 2004. Application of combined ridge-stein estimator to linear pushbroom imagery exterior orientation, *Geomatics and Information Science of Wuhan University*, 29(10), pp. 893-896.

Satellite	Acquired Time	Incidence Angle (°)	Ground Spatial Resolution (m)	Projection
SPOT5	2002.2.10	2.76	5	Linear central projection
SPOT4	2005.4.27	15	10	Linear central projection
ERS-2	1998.9.2	22.9	along-track 12.5 across-track 12.5	Ground range projection
Radarsat-1	2002.11.6	44.3	along-track 8.82 across-track 5.56	Slant range projection

Table 2. Statistics of attributes of four space-borne images

Stereo Models	RMS_X (m)			RMS_Y (m)			RMS_Z (m)		
	Min	Max	Mean	Min	Max	Mean	Min	Max	Mean
Radarsat1-ERS2	3.93	46.00	20.56	0.32	72.45	26.45	0.10	46.61	15.96
Radarsat1-SPOT4	1.48	24.56	12.59	0.07	46.54	15.21	0.62	37.78	20.91
SPOT4-ERS2	1.56	26.74	10.83	0.90	40.12	15.26	0.62	53.86	21.41
SPOT5-ERS2	0.11	25.22	10.85	0.64	31.00	12.55	0.02	50.67	21.00
SPOT5-Radarsat1	0.08	25.67	10.67	0.76	29.49	12.37	0.85	40.88	21.26
SPOT5-SPOT4	1.23	23.90	10.73	1.29	35.74	13.02	0.03	64.34	28.24

Table 3. Statistics of RMS of composite stereo positioning

Stereo Models	Overlap (%)	Intersection Angle (o)	Length of Baseline (m)	Flying Height (m)	Base-height Ratio (m)
Radarsat1-ERS2	100	68.59	1095151.67	769033	1.44
Radarsat1-SPOT4	50	61.09	990691.93	793616	1.30
SPOT4-ERS2	85	8.68	131293.81	803668	0.16
SPOT5-ERS2	100	27.84	410291.37	781386	0.52
SPOT5-Radarsat1	90	40.75	690107.92	771334	0.90
SPOT5-SPOT4	60	20.61	305751.73	805969	0.37

Table 4. Statistics of attributes of stereoscopic pairs